# B cell homeostasis and follicle confines are governed by fibroblastic reticular cells

Viviana Cremasco[1,9], Matthew C Woodruff[2,3,9], Lucas Onder[4], Jovana Cupovic[4], Janice M Nieves-Bonilla[1], Frank A Schildberg[1], Jonathan Chang[1,3], Floriana Cremasco[1,5], Christopher J Harvey[1], Kai Wucherpfennig[1], Burkhard Ludewig[4], Michael C Carroll[2,6] & Shannon J Turley[1,7,8]

Fibroblastic reticular cells (FRCs) are known to inhabit T cell–rich areas of lymphoid organs, where they function to facilitate interactions between T cells and dendritic cells. However, *in vivo* manipulation of FRCs has been limited by a dearth of genetic tools that target this lineage. Here, using a mouse model to conditionally ablate FRCs, we demonstrated their indispensable role in antiviral T cell responses. Unexpectedly, loss of FRCs also attenuated humoral immunity due to impaired B cell viability and follicular organization. Follicle-resident FRCs established a favorable niche for B lymphocytes via production of the cytokine BAFF. Thus, our study indicates that adaptive immunity requires an intact FRC network and identifies a subset of FRCs that control B cell homeostasis and follicle identity.

Secondary lymphoid organs are essential sites for the induction of adaptive immune responses. One of their most notable features is the segregation of B cells and T cells into discrete domains that consitute structural and functional units for optimal activation of cells of the immune system[1,2]. These specialized environments are inhabited by different subsets of mesenchymal stromal cells, which are commonly viewed as serving a scaffolding function for T lymphocytes, B lymphocytes and dendritic cells. Current dogma holds that fibroblastic reticular cells (FRCs) within the paracortical region coordinate T cell responses, whereas follicular dendritic cells (FDCs) within the cortex support B cell responses. However, precise understanding of how the stromal network of lymphoid organs controls adaptive immunity has not been achievable due to limitations in technology for targeting each of the mesenchymal cell populations.

The T cell paracortical region of the lymph node is delineated by FRCs, the most abundant population of nonhematopoietic or stromal cells in this organ. Typified by expression of the glycoprotein podoplanin (PDPN) and receptors for platelet-derived growth factor, such as CD140α and CD140β, FRCs construct an elaborate conduit network that allows small molecules to flow rapidly from upstream tissues deep into the parenchyma of lymph nodes[3–5]. Expression of the chemokines CCL19 and CCL21 by FRCs, in addition to the expression of other adhesion molecules, facilitates chemokine receptor CCR7–dependent homing of naive T cells and provides essential guidance cues to dendritic cells that migrate from nonlymphoid tissues into the lymph node paracortex[6–8]. Additionally, the production of interleukin 7 (IL-7) by FRCs is thought to be essential for preservation of the peripheral T cell pool under homeostatic conditions[9]. FRCs have also been found to control the extent of proliferation of newly activated T cells through the regulated release of nitric oxide[10–12].

The two stromal cell populations commonly characterized within the lymph node cortex include FDCs and marginal reticular cells (MRCs). FDCs are characterized by localization within B cell follicles, expression of the complement receptors CR1 (CD35) and CR2 (CD21) and the FDC marker FDCM1 and the ability to display opsonized antigens to B cells. Expression of B cell–trophic factors (the chemokine CXCL13 and the prosurvival factor BAFF (also known as BlyS, TALL-1, TNFSF13B or TNFSF20)) is often attributed to FDCs, which links these cells to shepherding B cells to follicles, supporting B cell survival and coordinating the germinal center reaction[13–16]. Published work using a system to ablate FDCs has provided definitive evidence that although this stromal subset is critical for germinal center responses, it has only a minor role in B cell homeostasis within resting lymph nodes[17]. Likewise, loss of FDCs is not mirrored by a decrease in the abundance of transcripts encoding BAFF (*Tnfsf13b*; called '*Baff*' here), which indicates the presence of an alternative source. Such observations have led some investigators to postulate that MRCs, which reside in close proximity to the subcapsular sinus of lymph nodes[18], serve these functions. However, data supporting this hypothesis are not yet available, so the cell population that supports B cell homeostasis within primary follicles has remained unconfirmed.

[1]Department of Cancer Immunology and AIDS, Dana Farber Cancer Institute, Boston, Massachusetts, USA. [2]Program in Cellular and Molecular Medicine, Children's Hospital, Boston, Massachusetts, USA. [3]Division of Medical Sciences, Harvard Medical School, Boston, Massachusetts, USA. [4]Institute of Immunobiology, Kantonal Hospital St. Gallen, St. Gallen, Switzerland. [5]Department of Pharmacology, University of Milan, Milan, Italy. [6]Department of Pediatrics, Harvard Medical School, Boston, Massachusetts, USA. [7]Department of Microbiology and Immunobiology, Harvard Medical School, Boston, Massachusetts, USA. [8]Present address: Genentech, South San Francisco, California, USA. [9]These authors contributed equally to this work. Correspondence should be addressed to S.J.T. (turley.shannon@gene.com) or M.C.C. (michael.carroll@childrens.harvard.edu).

We have developed and experimentally confirmed an inducible mouse model for conditional ablation of FRCs *in vivo* by crossing mice with transgenic expression of Cre recombinase directed by the *Ccl19* promoter (*Ccl19*-Cre mice) with mice expressing the receptor for diphtheria toxin (DTxn) from the ubiquitous *Rosa26* locus (*Rosa26*-iDTR mice). In the *Ccl19*-Cre × iDTR progeny, administration of DTxn caused rapid and extensive depletion of FRCs but spared other stromal cell populations. Our data demonstrate that ablation of FRCs led to marked alterations in the homeostasis and compartmentalization of T cells, with profound consequences for the activation, population expansion and effector function of viral antigen–specific T lymphocytes. Unexpectedly, the loss of FRCs also led to substantially reduced B cell viability and altered follicular organization, followed by marked impairment in humoral immunity to T cell–dependent and T cell–independent viral antigens. Mechanistically, we determined that a subset of FRCs residing within lymphoid follicles established a favorable niche for B lymphocytes via production of BAFF.

Collectively, our results demonstrate that FRCs are required for the generation of virus-specific T cell responses within lymphoid organs. Additionally, our study broadens the current paradigm that FRCs support solely T cell immunity. In doing so, it highlights an essential role for FRCs in directly controlling the homeostasis, distribution and activation of B cells.

## RESULTS

### *In vivo* genetic targeting and selective ablation of FRCs

The manipulation of FRCs *in vivo* has thus far been limited by a lack of specific genetic models that target this population of stromal cells. To address this limitation, a *Ccl19*-Cre mouse line has been generated that permits targeting of FRCs[19]. By crossing the *Ccl19*-Cre line to a line of mice expressing enhanced yellow fluorescent protein (eYFP) from the *Rosa26* locus (*Rosa26*-eYFP), we generated *Ccl19*-Cre × *Rosa26*-eYFP reporter mice in which eYFP expression is achieved following Cre-mediated excision of a *lox*P-flanked transcriptional 'stop' sequence (**Supplementary Fig. 1a**). Confocal laser-scanning microscopy of lymph nodes from *Ccl19*-Cre × *Rosa26*-eYFP mice revealed expression of the *Ccl19*-Cre transgene in the T cell zone (**Fig. 1a,b**), which supported the conclusion of efficient excision of *lox*P-flanked loci in the expected location. Flow cytometry demonstrated eYFP expression in FRCs, identified as nonhematopoietic cells that expressed PDPN and were negative for the endothelial marker CD31 and the cell-adhesion molecule MadCAM-1 (CD45⁻PDPN⁺CD31⁻MadCAM⁻) (**Fig. 1c** and **Supplementary Fig. 1b**). We did not detect eYFP expression in other lymph node stromal cells, including lymphatic endothelial cells (CD45⁻PDPN⁺CD31⁺), blood endothelial cells (CD45⁻PDPN⁻CD31⁺) or integrin α₇–expressing pericytes (CD45⁻PDPN⁻CD31⁻) (**Fig. 1c**), which confirmed the specificity of the *Ccl19* promoter. Despite published reports suggesting a close developmental relationship between FRCs and MRCs (CD45⁻PDPN⁺CD31⁻MadCAM⁺)[20], MRCs did not seem to be targeted by the *Ccl19*-directed Cre recombinase, as

demonstrated by flow cytometry and confocal microscopy showing the absence of eYFP expression in MadCAM-1⁺ cells lining the subcapsular sinus (**Fig. 1c–e**).

To generate a mouse model that enables selective depletion of FRCs, we crossed mice with the gene encoding the simian DTR downstream of a *lox*P-flanked transcriptional stop element in the *Rosa26* locus[21] to *Ccl19*-Cre mice (**Supplementary Fig. 1c**). In the resulting progeny, cells with an active *Ccl19* promoter (FRCs) express the simian DTR and are selectively vulnerable to toxin-induced apoptosis when exposed to DTxn. A single injection of DTxn into these mice was sufficient to achieve rapid and extensive ablation of FRCs from lymph nodes (**Fig. 2a–c**). FRCs were lost as early as 24 h following the administration of DTxn (**Fig. 2a–c**), and the deletion was specific, as we did not detect changes in cellularity of other lymph node stromal populations, including lymphatic endothelial cells, blood endothelial cells and integrin α₇–expressing pericytes (**Fig. 2d**). Consistent with FRCs' being the predominant source of CCL19 (refs. 8,9), expression of *Ccl19* in lymph nodes was abrogated after ablation of FRCs, whereas expression of genes shared with other cells, such as *Ccl21* (ref. 8), was only partially reduced (**Fig. 2e,f**). Thus, we were able to detect MadCAM-1⁺RANKL⁺ cells along the lymph node subcapsular sinus of mice that had undergone ablation of FRCs (**Fig. 2g** and **Supplementary Fig. 1d**), which confirmed a lack of *Ccl19* promoter activity in MRCs. In line with that finding, the abundance of transcripts encoding the cytokine RANKL (*Tnfsf11*), which is shared by MRCs and FRCs[8,18], was reduced only partially in total lymph node mRNA preparations after ablation of FRCs (**Supplementary Fig. 1e**), despite complete abrogation of *Ccl19* expression (**Fig. 2e**).

Despite the fact that FRCs constitute a very small cellular compartment (~0.5% of total lymph node cells)[22], their ablation resulted in considerable alterations in the lymph nodes, with significant reductions in the size, weight and cellularity of the lymph nodes (**Fig. 3a,b**
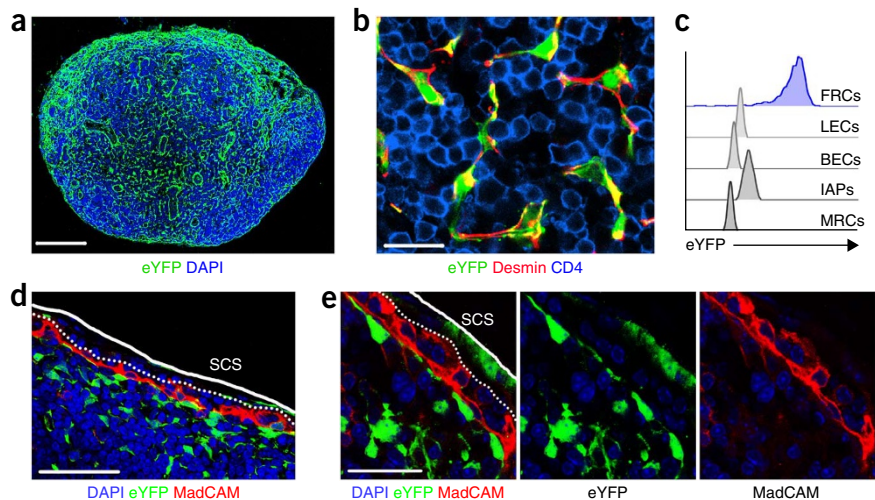


**Figure 1** Specific *Ccl19* promoter activity in FRCs. (**a**) Microscopy of a section of a popliteal lymph node from a *Ccl19*-Cre × *Rosa26*-eYFP reporter mouse, stained with an antibody to GFP (anti-GFP) that also stains eYFP and with the DNA-binding dye DAPI. Scale bar, 200 μm. (**b**) Enlargement of the paracortical area of a section as in **a**, stained for GFP, desmin and CD4. Scale bar, 25 μm. (**c**) Flow cytometry of freshly isolated stromal cells from *Ccl19*-Cre × *Rosa26*-eYFP mice, showing *Ccl19* promoter activity via expression of eYFP. LECs, lymphatic endothelial cells; BECs, blood endothelial cells; IAPs, integrin α₇-expressing pericytes. (**d,e**) Confocal microscopy of lymph nodes from *Ccl19*-Cre × *Rosa26*-eYFP mice, stained with DAPI, anti-GFP and anti-MadCAM, showing the ceiling (solid lines) and floor (dotted lines) of the subcapsular sinus (SCS). Scale bars, 50 μm (**d**) and 25 μm (**e**). Data are representative of three independent experiments with more than three mice (**a,b,d,e**) or two independent experiments with three mice (**c**).

**Figure 2** Conditional ablation of FRCs. (a) Identification of the FRC (PDPN+CD31−) compartment (top left quadrant) in *Ccl19*-Cre × iDTR mice 24 h after the administration of DTxn. DTR+Cre+ mice express DTR in *Ccl19*-expressing cells, whereas DTR+Cre− control mice lack DTR due to the absence of Cre expression. Numbers in quadrants indicate percent cells in each. (b,c) Frequency of FRCs among stromal (CD45−) cells (b) and total FRCs per lymph node (LN) (c) in mice as in a at 12–72 h (horizontal axis) after administration of DTxn. (d) Flow cytometry of stromal cells in lymph nodes collected from *Ccl19*-Cre DTR+Cre+ and DTR+Cre− mice 72 h after injection of DTxn: FRCs, CD45−PDPN+CD31−; lymphatic endothelial cells, CD45−PDPN+CD31+; blood endothelial cells, CD45−PDPN−CD31+; integrin α7−expressing pericytes, CD45−PDPN−CD31−. (e,f) Abundance of *Ccl19* transcripts (e) and *Ccl21* transcripts (f) in lymph nodes from mice as in a at 24, 28 or 72 h (horizontal axes) after administration of DTxn; results are normalized to those of the gene encoding cyclophillin. Each symbol represents one lymph node from an individual mouse (n = 4–10 per group); small horizontal lines indicate the mean. (g) Microscopy of MRCs in lymph nodes obtained from *Ccl19*-Cre DTR+Cre+ and DTR+Cre− mice at 24 h after treatment with DTxn, identified by staining with anti-MadCAM, together with DAPI and anti-desmin; middle (insets), enlargement of areas outlined in main images. Scale bars, 200 μm (main images) or 100 μm (insets). NS, not significant; *P < 0.05, **P < 0.01 and ***P < 0.001 (Student's t-test). Data are representative of at least three independent experiments with four (a–c) or three (d) mice per group in each (mean and s.d.), two to three experiments (f) or three independent experiments with over three mice (g).
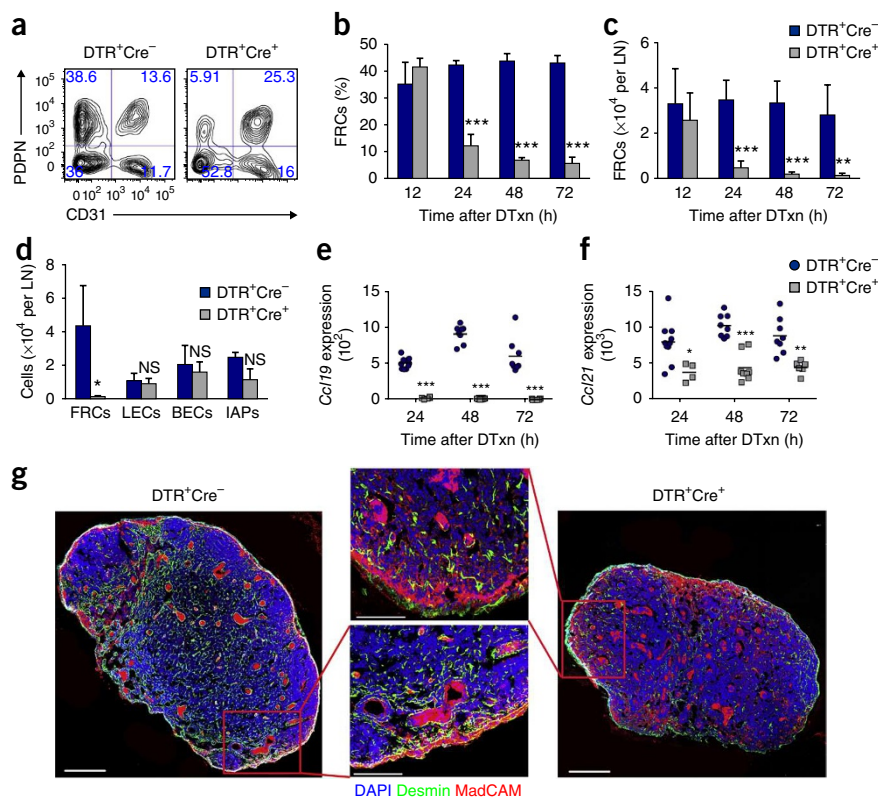
and data not shown). However, those effects were not symptomatic of a global collapse of lymph node architecture, as ablation of FRCs perturbed neither the integrity nor the permeability of the conduit network (**Fig. 3c**). The administration of DTxn was not associated with systemic toxicity, and it did not lead to weight loss or extranodal pathology (**Supplementary Fig. 2a** and data not shown). Furthermore, we did not observe accumulation of either neutrophils (CD11b+Gr1hi) or monocytes (CD11b+Gr1− or CD11b+Gr1lo) or increased expression of inflammatory cytokines (**Supplementary Fig. 2b,c**), which

ruled out the possibility of extraneous inflammation secondary to the ablation of FRCs. Collectively, these data suggested that the *Ccl19*-Cre mouse system allowed specific ablation of FRCs *in vivo*.

### Ablation of FRCs impairs antiviral T cell responses

Confocal laser-scanning microscopy of *Ccl19*-Cre × iDTR mice treated with DTxn confirmed the disappearance of FRCs from the T cell zone parenchyma and revealed aberrant localization of T lymphocytes within cortical regions (**Fig. 4a**). Notably, we also observed a global reduction in the number of T cells in lymph nodes (**Fig. 4b**), with CD4+ T cells and CD8+ T cells affected equally by the loss of FRCs (**Supplementary Fig. 3a,b**). Moreover, expression of the gene encoding the T cell–survival factor IL-7 was also reduced in lymph nodes from mice in which FRCs were ablated (**Fig. 4c**), which suggested that diminished T cell viability may have compounded the reduction in T cell numbers. To assess the effect of ablation of FRCs in adaptive T cell responses, we immunized *Ccl19*-Cre × iDTR mice with a replication-incompetent influenza A virus expressing the OT-II ovalbumin peptide and monitored the generation of antigen-specific
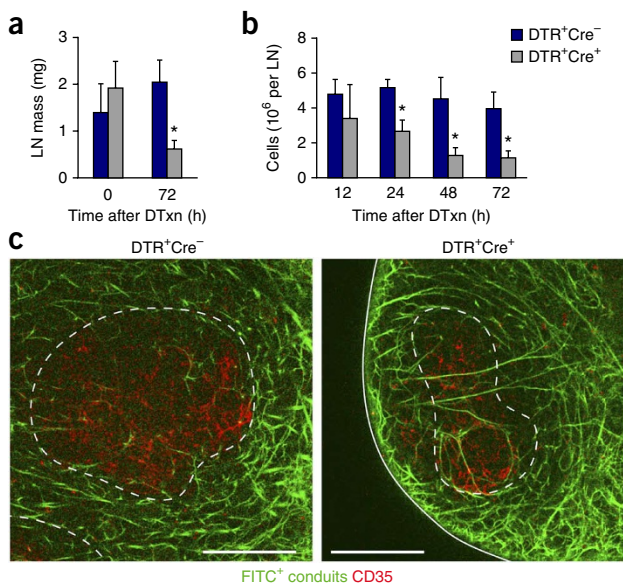


**Figure 3** Ablation of FRCs has profound consequences on lymph node cellularity despite preserving conduit functionality. (a,b) Lymph node mass (a) and total cellularity of lymph nodes (b) in *Ccl19*-Cre DTR+Cre+ and DTR+Cre− mice (as in **Fig. 2a**) at various times (horizontal axes) after administration of DTxn. (c) Multiphoton microscopy of popliteal nodes from *Ccl19*-Cre DTR+Cre+ and DTR+Cre− mice showing transport of a fluorescein isothiocyanate (FITC)-tagged tracer into conduits, plus staining with anti-CD35; dashed lines outline B cell follicles. Scale bars, 100 μm. *P < 0.001 (Student's t-test). Data are representative of at least two independent experiments with three mice per group in each (a,b; mean and s.d.) or two independent experiments with more than three mice (c).
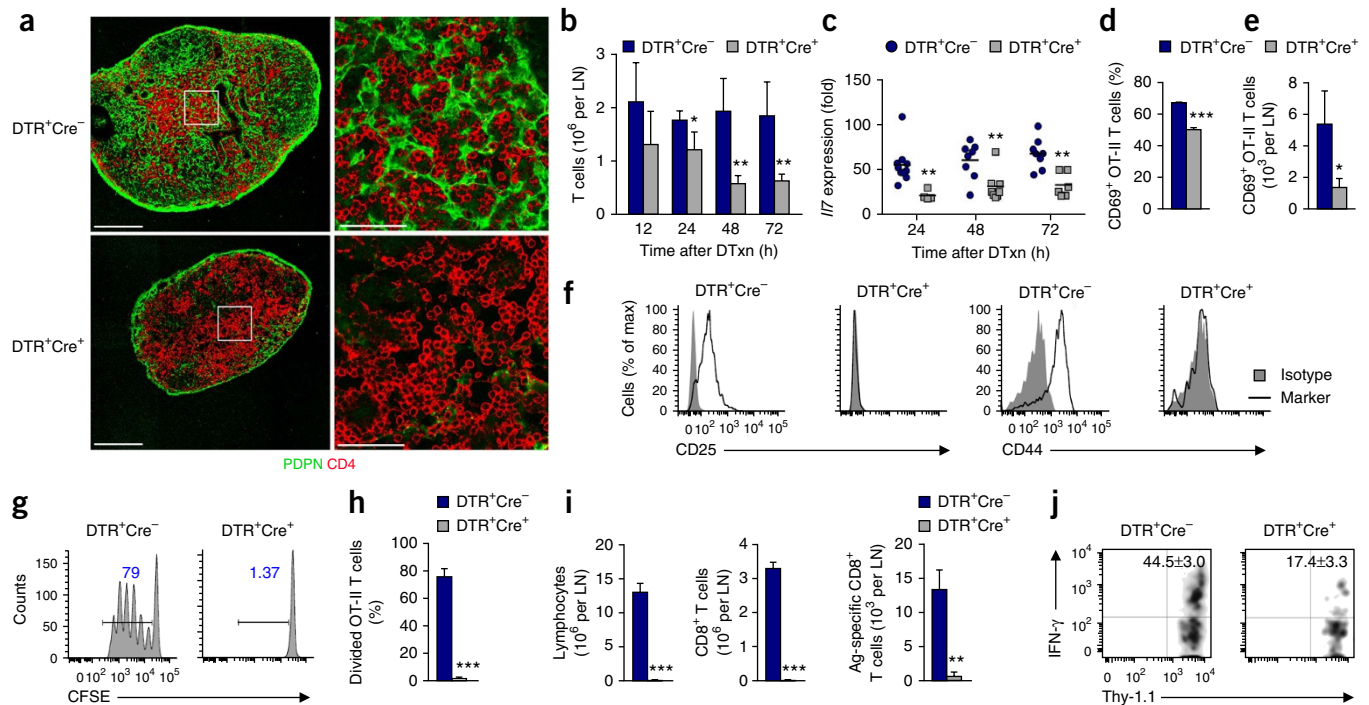
**Figure 4** Ablation of FRCs impairs T cell immunity. (**a**) Confocal microscopy of lymph node sections obtained from *Ccl19*-Cre DTR+Cre+ and DTR+Cre− mice 3 d after treatment with DTxn and stained with anti-CD4 (T cells) and anti-PDPN (FRCs) to detect FRCs in paracortical areas; right, enlargement of areas outlined at left. Scale bars, 200 μm (left) or 50 μm (right). (**b**) Quantification of T cells (CD45+B220−CD3+) in skin-draining lymph nodes from *Ccl19*-Cre DTR+Cre+ and DTR+Cre− mice at 3 d after treatment with DTxn, assessed by flow cytometry. (**c**) Abundance of *Il7* transcripts in lymph nodes from *Ccl19*-Cre DTR+Cre+ and DTR+Cre− mice (*n* = 4–10 per group) at 3 d after treatment with DTxn (presented as in **Fig. 2e,f**). (**d,e**) Frequency (**d**) and total number (**e**) of antigen-specific activated donor T cells (CFSE+CD3+CD4+V$_\alpha$5+CD69+) in popliteal nodes from *Ccl19*-Cre DTR+Cre+ and DTR+Cre− host mice (*n* = 3 per group) treated with DTxn, then given adoptive transfer of CFSE-labeled OT-II T cells and then immunized in the footpad with ovalbumin-expressing, ultraviolet irradiation–inactivated influenza virus, assessed by flow cytometry 24 h after immunization. (**f**) Expression of CD25 and CD44 in antigen-specific T cells, assessed by flow cytometry 60 h after immunization as in **d,e**. Isotype, isotype-matched control antibody. (**g**) Proliferation of OT-II T cells from mice as in **f**. Numbers above bracketed lines indicate percent cells with CFSE dilution (i.e., cells that have proliferated). (**h**) Summary of results in **g** (*n* = 3 per group). (**i**) Quantification of lymphocytes, CD8+ T cells and antigen (Ag)-specific T cells in *Ccl19*-Cre DTR+Cre+ and DTR+Cre− host mice (*n* = 3 per group) treated with DTxn, then given CD8+ T cells specific for the coronavirus spike protein before immunization with nonreplicating coronavirus particles, assessed 72 h after virus injection. (**j**) Intracellular staining of IFN-γ in mice as in **i** (*n* = 3 per group), assessed by flow cytometry. Numbers in top right quadrants indicate percent IFN-γ+ Thy-1.1+ (donor) cells (mean ± s.d.). *$P < 0.05$, **$P < 0.01$ and ***$P < 0.001$ (Student's *t*-test). Data are representative of three independent experiments with more than three mice (**a**), at least three independent experiments with four mice per group in each (**b**; mean and s.d.), at least three independent experiments experiments (**c**), two experiments with two to five mice per group (**d–h**; mean and s.d.) or one experiment with three mice (**i,j**; mean and s.d.).

T effector cells (**Supplementary Fig. 3c,d**). Loss of FRCs resulted in diminished priming of antigen-specific T cells (**Fig. 4d,e**), as well as reduced activation and proliferation (**Fig. 4f–h**). Furthermore, we observed a deterioration of antiviral T cell responses in a coronavirus-based vector system[23] in which we monitored the generation and effector function of exogenously transferred CD8+ T cells with transgenic expression of a T cell antigen receptor specific for the coronavirus spike protein before immunization with coronavirus vectors[24] (**Supplementary Fig. 3e**). Strikingly, generation of the virus-specific T cell response was also profoundly disrupted, with reduced numbers of antigen-specific CD8+ T cells and defective interferon-γ production in mice in which FRCs were ablated (**Fig. 4i,j**). Together our data demonstrated a critical role for FRCs in the homeostasis, positioning and activation of T cells.

## Ablation of FRCs is detrimental to B cells

Unexpectedly, we also observed a substantial reduction in the abundance of lymph node B cells following the administration of DTxn (**Fig. 5a,b**). We also observed structural alterations in the lymph node cortex, with reduced follicle size (**Fig. 5c**) and a loss of follicle boundaries (**Fig. 5d**). Ultimately, this resulted in an unfurling of the B cell

zone with mixing of B lymphocytes and T lymphocytes throughout the cortex (**Fig. 5d**). Notably, we detected no *Ccl19* promoter activity or intrinsic toxicity of DTxn in B lymphocytes (**Supplementary Fig. 3f,g**), which suggested a physiological relationship between B cell homeostasis and the presence of FRCs.

To determine the functional consequences of the aberrant follicular architecture and decreased B cell numbers, we ablated FRCs in mice and assessed the ability of the mice to mount a humoral response to influenza A virus. Immunization with influenza virus inactivated by ultraviolet irradiation resulted in a disorganized accumulation of B cells in the ensuing germinal center response (**Fig. 5e**), as well as a significant reduction in the production of influenza-specific immunoglobulin M (IgM) (T cell–independent antibody[25]) and IgG2b (T cell–dependent antibody) (**Fig. 5f**).

The detrimental effect of ablation of FRCs on B cells was not restricted to lymph nodes. In splenic white pulp, where the *Ccl19* promoter was active in both FRCs and CD31−PDPN− (double-negative) cells[19] (**Supplementary Fig. 4a**), the administration of DTxn efficiently targeted eYFP+ stroma (**Supplementary Fig. 4b,c**), with a substantial decrease in the abundance of FRCs and CD31−PDPN− (double-negative) cells (**Supplementary Fig. 4d,e**).

**Figure 5** Ablation of FRCs is detrimental to B cells. (**a**,**b**) Frequency of B cells (CD45+B220+CD3−) among hematopoietic (CD45+) cells (**a**) and total B cells (**b**) in skin-draining lymph nodes from *Ccl19*-Cre DTR+Cre+ and DTR+Cre− mice, assessed by flow cytometry. (**c**,**d**) Follicle size (**c**) and architecture (**d**) in lymph node sections from *Ccl19*-Cre DTR+Cre+ and DTR+Cre− mice (*n* = 3 (**c**) or *n* > 3 (**d**)) at 3 d after injection of DTxn, assessed by staining with anti-B220 (B cells (B)) and anti-CD4 (T cells (T)). Solid lines (**d**), lymph node capsule; dashed lines (**d**), cortical-paracortical boundary. Scale bars (**d**), 100 μm. (**e**) Microscopy of germinal centers (GC) in popliteal nodes from *Ccl19*-Cre DTR+Cre+ and DTR+Cre− mice 14 d after immunization with influenza virus, stained with anti-B220 (B cells), anti-GL7 (activated B cells) and anti-CD35 (FDCs). Scale bars, 100 μm. (**f**) Enzyme-linked immunosorbent assay of IgM and IgG2b influenza virus–specific antibodies in serum from mice as in **e**, assessing T cell–independent and T cell–dependent humoral responses, respectively. *P < 0.05, **P < 0.01 and ***P < 0.001 (Student's *t*-test). Data are representative of at least three independent experiments with four mice per group in each (**a**,**b**; mean and s.d.), three independent experiments (**c**,**d**; mean and s.d. in **c**), three experiments (**e**) or two independent experiments with three to five mice per group in each (**f**; mean and s.d.).
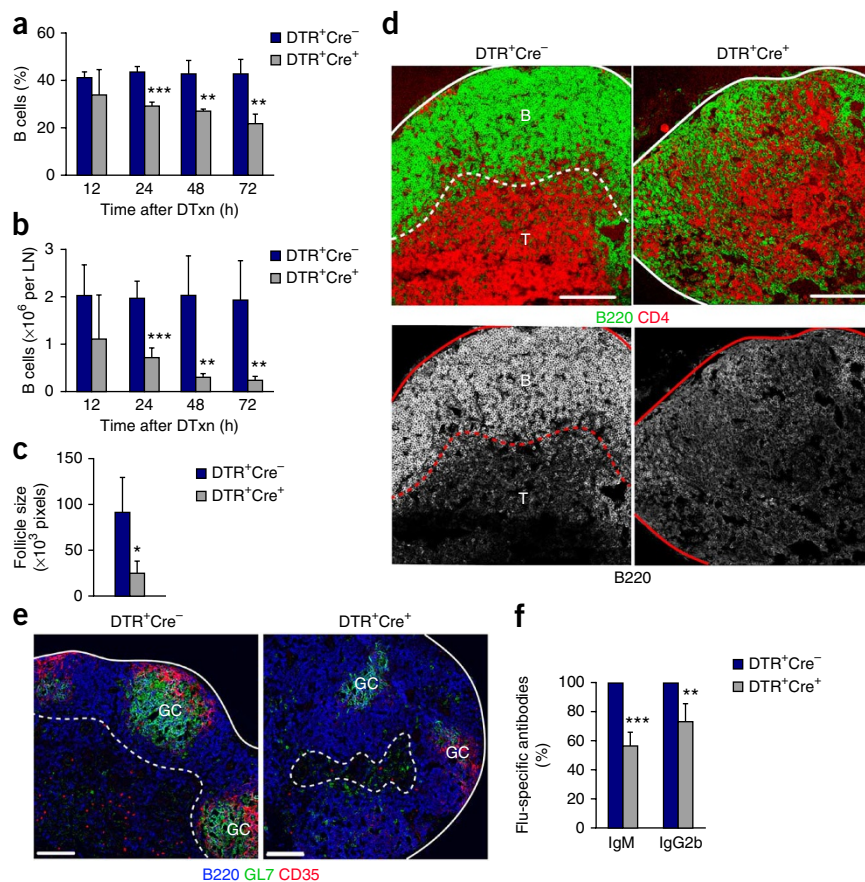


The ablation of FRCs had no effect on splenic weight or cellularity (**Supplementary Fig. 4f,g**) but markedly altered white pulp architecture (**Supplementary Fig. 4h**). B cell numbers were also reduced in the spleen (**Supplementary Fig. 4i**), although to a lesser extent than in lymph nodes (**Supplementary Fig. 4j**). Functionally, the effects observed in the spleen affected marginal zone humoral responses, with a significant decrease in IgM production upon immunization with the antigen TNP-Ficoll (2,4,6-trinitrophenyl linked to the hydrophilic polysaccharide Ficoll) (**Supplementary Fig. 4k**). As the *Ccl19* promoter was also active in Peyer's patches[19] (**Supplementary Fig. 5a**), we investigated the fate of Peyer's patches following the ablation of FRCs. Systemic administration of DTxn elicited less substantial disruption of populations in Peyer's patches than in the spleen or lymph nodes, with smaller reductions in the number of FRCs and B cells than those in the spleen or lymph nodes (**Supplementary Fig. 5b,c**). Similarly, we observed no major anatomical alterations, with the exception of a paucity of T cell clusters in interfollicular regions (**Supplementary Fig. 5d**). Together these observations indicated an unanticipated regulation of B cell homeostasis by FRCs and suggested that damage to the FRC network had deleterious consequences on the cellular circuitries that underpin humoral responses.

### Lymph node FRCs support the homing and survival of B cells

Given the reported role of FRCs in regulating the trafficking of cells of the immune system[6,7,9,26], we hypothesized that the decrease in B cell numbers after the ablation of FRCs might have stemmed from impaired homing of lymphocytes to lymph nodes. To test this hypothesis, we labeled congenic B cells with the division-tracking dye CFSE and adoptively transferred the cells into DTxn-treated *Ccl19*-Cre × iDTR mice, then counted the transferred cells in lymph nodes

90 min and 24 h later by flow cytometry. Donor B cell numbers were markedly reduced at both time points in the lymph nodes of mice in which FRCs were ablated (**Supplementary Fig. 6a**). The homing of B cells to lymph nodes depends on the chemokines CCL19 and CXCL12 (ref. 27), and *Cxcl12* expression in FRCs has been documented[8]. Indeed, *Cxcl12* expression was considerably reduced in mice in which FRCs were ablated (**Supplementary Fig. 6b**), and FRCs were sufficient to elicit B cell chemotaxis *in vitro* (**Supplementary Fig. 6c**), which suggested that FRCs recruited B cells, possibly via CXCL12 and CCL19. Notably, blockade of lymphocyte ingress (via treatment with an antibody that blocks the lymph node–homing receptor CD62L) was not sufficient to appreciably perturb B cell numbers in the first 24 h after treatment (**Supplementary Fig. 6d**), in contrast to the rapid B cell loss observed in mice in which FRCs were ablated (**Fig. 5a,b**). Additionally, preventing the egress of lymphocytes from lymph nodes with FTY720 (an antagonist of the receptor for sphingosine 1-phosphate) did not completely restore B cell numbers following ablation of FRCs (**Supplementary Fig. 6e**). Together these data suggested that while B cell entry required an intact FRC network, impaired B cell trafficking accounted for only part of the reduction in B cell numbers following the ablation of FRCs. That consideration prompted us to investigate the possibility that FRCs might regulate additional aspects of B cell homeostasis. Consistent with this hypothesis, B cell loss in mice in which FRCs were ablated coincided with a significant increase in propidium iodide–positive B cells (**Fig. 6a,b**), which linked FRCs to the promotion of B cell survival.

### Ablation of FRCs impairs BAFF production *in vivo*

Most efforts to characterize FRCs have thus far focused on their roles in supporting the homeostasis, migration and activation of T cells.

**Figure 6** Ablation of FRCs impairs B cell survival. (**a,b**) Frequency of viable B cells in single-cell suspensions of lymph nodes from *Ccl19*-Cre DTR+Cre+ and DTR+Cre− mice at 24 or 72 h (horizontal axis, **a**) or 72 h (**b**) after treatment with DTxn, assessed by staining with propidium iodide (PI) followed by flow cytometry. Numbers adjacent to outlined areas (**b**) indicate percent dying (PI+) B cells (CD45+B220+). (**c**) Confocal microcopy of lymph nodes from *Ccl19*-Cre × *Rosa26*-eYFP mice (*n* > 3), showing FRCs in follicular regions (lines as in **Fig. 5d**); right, enlargement (2.9×) of areas outlined at left. B, B cell follicle. Scale bar, 50 µm. (**d**) Confocal microcopy of a popliteal lymph node from a *Ccl19*-Cre × *Rosa26*-eYFP mouse, stained with anti-FDCM1, anti-CXCL13, anti-GFP and anti-CCL21 to detect chemokine expression (left) and FDCs (middle); right, single channels of the follicle area outlined at left (lines as in **Fig. 5d**). Scale bar, 100 µm (left), enlargement, 1.9× (middle) and 4.75× (right). (**e**) Confocal microscopy of popliteal lymph nodes from a *Ccl19*-Cre DTR+Cre− mouse left untreated and from *Ccl19*-Cre DTR+Cre+ mice at 24, 48, or 72 h (above images) after administration of DTxn, stained with anti-FDCM1 to detect FDCs. Scale bar, 200 µm. (**f**) Cumulative FDCM1 expression in follicles in images as in **e**. Each symbol represents one lymph node from an individual mouse. AU, arbitrary units. (**g,h**) *Baff* expression (**g**) and quantification of B cells (**h**) in *Ccl19*-Cre (DTR+Cre+ and DTR+Cre−) mice, in which FRCs were targeted, and *Cd21*-Cre mice (DTR+Cre+ and DTR+Cre−) mice, in which FDCs were targeted, at 24 h after treatment with DTxn (presented as in **Fig. 2e,f**). (**i,j**) Abundance of *Baff* transcripts (**i**) and *April* transcripts (**j**) in lymph nodes from *Ccl19*-Cre DTR+Cre+ and



DTR+Cre− mice (*n* = 6–8 per group) 3 d after administration of DTxn (presented as in **Fig. 2e,f**). (**k**) Confocal microscopy of lymph nodes from *Ccl19*-Cre DTR+Cre+ and DTR+Cre− mice in which FRCs were ablated, stained with anti-BAFF and DAPI. Scale bars, 50 µm. *$P < 0.05$, **$P < 0.01$ and ***$P < 0.001$ (Student's *t*-test). Data are representative of two independent experiments with three to five mice per group in each (**a,b**; mean and s.d. in **a**), three independent experiments with more than three mice (**c**), two independent experiments (**d**), three independent experiments with more than three mice per group (**e**), one experiment with more than three mice per group (**f**), one experiment with two to four mice per group (**g,h**; mean and s.d.), three independent experiments (**i,j**) or two independent experiments with two mice (**k**).
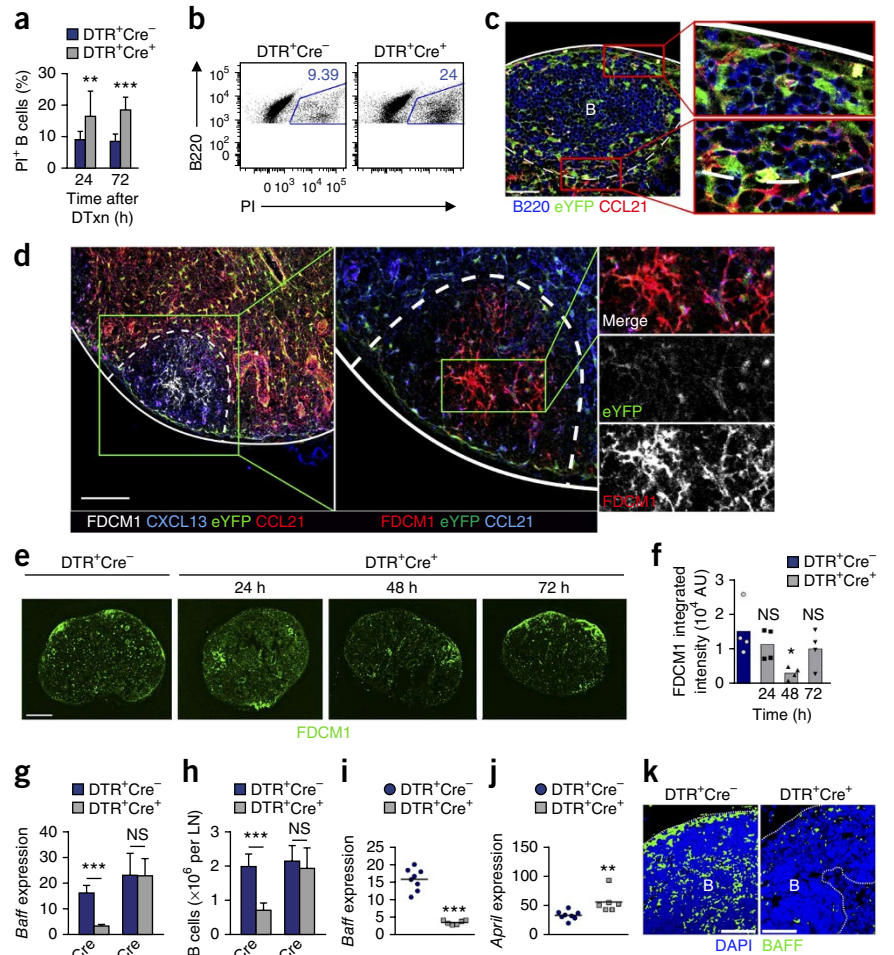
However, a discrete population of FRCs was also present in and around follicles (B cell zone FRCs; **Fig. 6c**), and we reasoned that such a locale could position FRCs to directly interact with and influence B cells. That observation, together with the decreased survival of B cells observed in mice in which FRCs were ablated, led us to hypothesize that FRCs might provide critical survival factors for naive B cells. In this context, BAFF has a critical role in survival of mature B cells[28,29]. The key source of BAFF in secondary lymphoid organs has been identified as a radiation-resistant cell[30], with FDCs often being considered the sole BAFF-producing stromal cell[31]. Thus, we reasoned that the phenotypes of mice in which FRCs were ablated might have been secondary to a decrease in the abundance or function of FDCs. To determine if FDCs were directly targeted in our system, we ascertained whether the *Ccl19* promoter was active in FDCs *in situ* by fluorescence imaging of *Ccl19*-Cre × *Rosa26*-eYFP mice. As shown by staining of the FDC marker FDCM1 and CXCL13, eYFP was absent from most FDCs in steady-state lymph nodes (**Fig. 6d**). We detected less staining of eYFP in a small number of FDCM1+ processes (**Fig. 6d**), possibly due to the tight interconnections that exist between FRCs and FDCs in follicles[4,32]. Additionally, to investigate the status of FDCs in mice

in which FRCs were ablated, we assessed lymph nodes by quantitative microscopy at various time points after the administration of DTxn. Our data demonstrated that FDCs were present 24 h after such treatment (**Fig. 6e**; quantification, **Fig. 6f**), despite profound loss of FRCs (**Fig. 2c**). Furthermore, FDCs remained functionally competent at this time point, as demonstrated by their ability to correctly display exogenous immunocomplexes (**Supplementary Fig. 7a**). Prolonged exposure to DTxn led to a progressive reduction in FDC volume, as shown by a decrease in the integrated intensity of FDCM1 staining (**Fig. 6e,f**) and decreased CD35 staining as well (data not shown). Notably, contraction of the FDC network appeared to be transient and was followed by the reappearance of FDCM1+ cells 3 d after ablation of FRCs (**Fig. 6e,f**). We next compared mice in which FRCs were ablated (*Ccl19*-Cre × iDTR mice treated with DTxn) with mice in which FDCs were ablated (lethally irradiated *Cd21*-Cre × iDTR mice reconstituted with wild-type bone marrow and treated with DTxn). Direct comparison of the ablation of FRCs and that of FDCs revealed that loss of FRCs rapidly abrogated *Baff* expression *in vivo*, while depletion of FDCs did not (**Fig. 6g**). Together these results indicated a previously unrecognized regulatory role for FRCs in maintaining the amount of

**Figure 7** FRCs support the survival of B cells through the production of BAFF. (**a**) Microscopy of BAFF (stained with anti-BAFF) in FRCs (eYFP⁺ cells stained with anti-GFP) in a lymph node from a *Ccl19*-Cre × *Rosa26*-eYFP mouse; right, single channels of image at left (enlargement, 2×). Solid line, lymph node capsule; dashed line, B cell follicle. Scale bar, 20 μm. (**b**) Production of BAFF (right) by FRCs (PI⁻CD45⁻PDPN⁺CD31⁻MadCAM⁻ cells) among freshly isolated lymph node stromal cells from naive C57BL/6 mice, assessed by flow cytometry. Numbers in outlined areas indicate percent PDPN⁺ cells (left) or BAFF⁺ FRCs (right). (**c**) Expression of canonical FRC markers (horizontal axes) in BAFF⁺ or BAFF⁻ FRCs (sorting, top left), assessed by flow cytometry. αSMA, α-smooth muscle actin; FAP, fibroblast-activation protein. (**d**) Viability of purified B cells cultured alone or in the presence of FRCs (+FRCs), assessed daily by quantification of PI⁻B220⁺ cells per well. (**e**) Viability of B cells cultured alone (No FRCs), in contact with FRCs (+FRCs), separated from FRCs by a Transwell filter (+FRCs (TW)) or with FRC-conditioned culture supernatant (+FRC sup), assessed at day 5 of culture. (**f**) Viability of B cells cultured with (FRC sup +) or without (FRC sup −) FRC-conditioned supernatant, with (α-BAFF +) or without (α-BAFF −) the addition of BAFF-neutralizing antibody, assessed by flow cytometry. Each symbol (**e,f**) represents an individual well. *P < 0.001 (Student's *t*-test). Data are representative



of two independent experiments with three mice (**a**), three independent experiments with more than six mice (**b**), two experiments (**c**) or three independent experiments (**d**–**f**; mean and s.e.m. (**d**) or mean and s.d. (**e,f**) of at least three wells per group in each experiment).
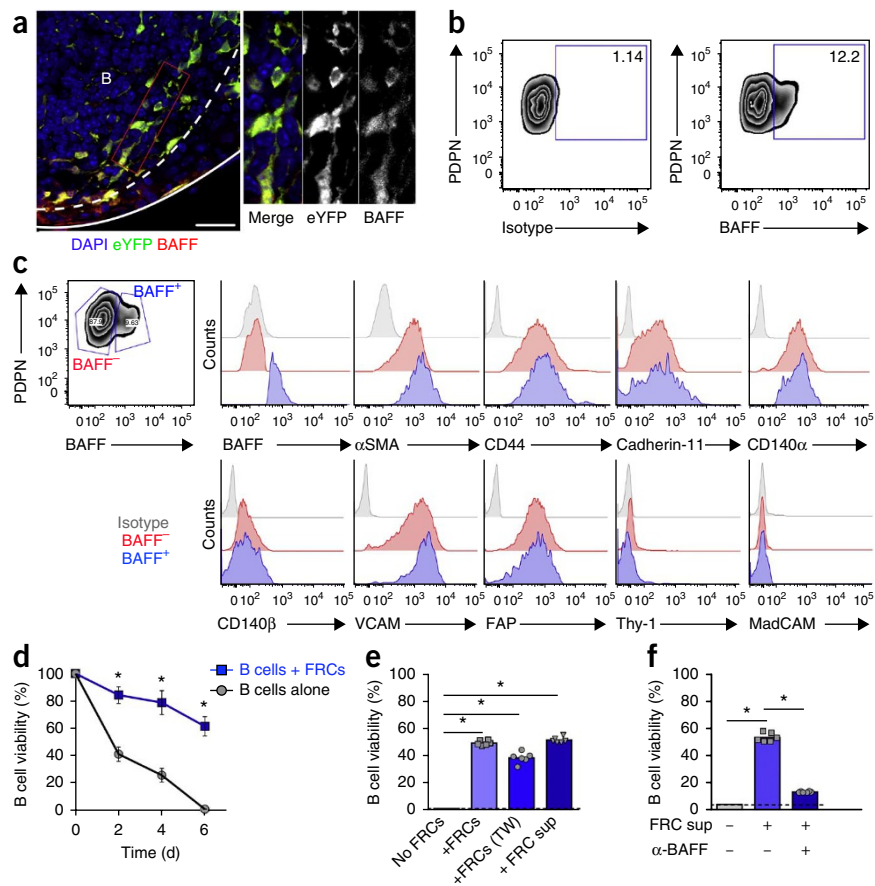
BAFF and the viability of B cells. Accordingly, we observed the large decrease in B cell numbers only in mice in which FRCs were ablated, not in mice in which FDCs were ablated (**Fig. 6h**). Notably, ablation of FRCs perturbed *Baff* expression without perturbing the expression of APRIL, a closely related member of the tumor-necrosis factor superfamily (encoded by *Tnfsf13*) (**Fig. 6i,j**). Moreover, the impaired expression of *Baff* mRNA in mice in which FRCs were ablated was mirrored by a similar abrogation in the abundance of BAFF protein, as assessed by confocal microscopy of lymph node sections (**Fig. 6k**). Notably, the concentration of BAFF in serum was unperturbed in mice in which FRCs were ablated (**Supplementary Fig. 7b**), which indicated that FRC loss influenced local BAFF production rather than perturbing a systemic reservoir. Furthermore, by injecting carefully 'titrated' DTxn into the footpad, we were able to achieve anatomically restricted ablation of FRCs and, consequently, B cell loss only in the draining popliteal lymph nodes without disrupting distal lymph nodes (**Supplementary Fig. 7c,d**). Thus, the functional consequences of FRC depletion on B cell homeostasis were mediated mainly by a local effect in the organ in which the ablation occurred.

**FRCs in the B cell zone constitute a chief source of BAFF**
The data shown so far suggested that FRCs might directly promote B cell survival by serving as a nonredundant source of BAFF, in agreement with published studies demonstrating expression of *Baff* mRNA in highly purified FRCs[8]. Confocal microscopy *in situ* of FRCs in the B cell zone revealed that these cells were indeed able to produce BAFF (**Fig. 7a**). In line with that finding, we also observed BAFF production

by flow cytometry in a discrete fraction of freshly isolated FRCs (**Fig. 7b**). Notably, BAFF was rapidly cleaved from the cell surface in a protease-dependent manner, similar to other molecules that belong to the tumor-necrosis factor superfamily (**Supplementary Fig. 7e**). BAFF⁺ cells were characterized by the expression of several canonical markers of FRCs, including PDPN, α-smooth muscle actin, CD44, cadherin-11, CD140α and CD140β, VCAM (the endothelial ligand for integrin α₄β₁) and fibroblast-activation protein (**Fig. 7c**), which supported the proposal that these cells were nearly identical to FRCs. Thus, our data suggested that FRCs positioned in follicular regions contributed to B cell homeostasis by providing the prosurvival factor BAFF. To directly test that hypothesis, we cultured B cells in the presence or absence of FRCs and measured B cell viability by staining the cells with propidium iodide, followed by flow cytometry. Notably, B cells cultured in the presence of FRCs exhibited significantly greater viability than that of B cells cultured alone (**Fig. 7d**). The elevated number of propidium iodide-negative B220⁺ cells in cultures with FRCs could not be accounted for by proliferation (**Supplementary Fig. 7f**). To ascertain whether the survival advantage conferred by FRCs was due to a soluble factor, we cultured B cells with stromal cells in separate compartments of a Transwell chamber or with FRC-conditioned medium. In both conditions, B cells exhibited enhanced viability (**Fig. 7e**), which indicated the presence of a soluble prosurvival factor derived from FRCs. Next we sought to determine whether the prosurvival factor contributed by FRCs was BAFF. For this, we preincubated FRC-conditioned medium with a BAFF-specific blocking antibody before adding the medium to B cells. Strikingly, the

enhancement of B cell survival was largely abrogated following neutralization of BAFF (**Fig. 7f**). In sum, our data have described a subset of FRCs that delineated the borders of B cell follicles in lymph nodes (FRCs in the B cell zone) and nurtured B cells through the production of BAFF (**Supplementary Fig. 8**).

## DISCUSSION

The absence of genetic tools for targeting FRCs has curbed the systematic *in vivo* assessment of their precise function in lymphoid organs. The generation of *Ccl19*-Cre mice has provided a solution to this technological limitation[19]. In particular, cell type–specific expression of DTR allowed us to assess the functional outcomes of disrupting the FRC network in physiological settings. The ablation of FRCs caused a substantial reduction in T cell numbers in resting lymph nodes and marked impairment in antigen-specific T cell responses. Unexpectedly, the ablation of FRCs was not immediately accompanied by collapse of the structured conduit system, which suggested that the lymph node infrastructure can persist and function despite a lack of support from stromal cells. In contrast, the absence of the cellular source of the reticular network (i.e., FRCs) affected the dynamics and function of T cells, which demonstrated that FRCs were essential for optimal T cell immunity but not for the short-term maintenance of the conduit system.

Using the genetic approach noted above, we made the unexpected observation that FRCs supported B cell homeostasis and the generation of humoral responses. While most lymph node FRCs reside in the T cell–rich paracortex, some localize to the vicinity of follicular conduits near the subcapsular sinus[4,32]. Our identification of *Ccl19*-Cre^{+} cells in B cell follicles (FRCs in the B cell zone) confirmed that FRCs span both the inner regions and the outer regions of the lymph node[33]. Unexpectedly, we found that FRCs in the B cell zone constituted a nonredundant source of BAFF. The source of BAFF in secondary lymphoid organs has been identified as a radioresistant cell[30] often attributed to FDCs. That concept has been confounded, however, by reports that abrogation of signaling via the receptor for lymphotoxin-β, which is critical for the development and maintenance of FDCs, does not affect BAFF expression or B cell numbers[34–37]. Further, a *Cd21*-Cre system for the conditional ablation of FDCs has provided evidence that these cells are dispensable for BAFF expression and the survival of naive B cells[17]. Although the possibility that FDCs contribute to BAFF production and their ablation induces compensatory upregulation by other cells cannot be excluded, these studies collectively have indicated an alternate source of BAFF in resting lymph nodes. On the basis of our data, we propose that FRCs in the B cell zone represent this source of BAFF and thereby directly support B cell homeostasis. The disrupted follicular organization in mice in which FRCs were ablated may have also contributed to decreased B cell survival, as FRCs in intact lymphoid organs would coordinate the migration of naive B cells from high endothelial venules to BAFF-rich follicles. Furthermore, while ablation of FRCs did not appear to impede the flow of lymph through the lymph node conduit network, it may have affected the ability of migratory dendritic cells to deliver tissue-derived antigens to T cells and B cells and thus may have contributed to the diminished antibody production observed in *Ccl19*-Cre × iDTR mice. Collectively, our findings indicated that alterations in lymph node stromal composition can have catastrophic consequences on immunological competence, with decreased lymphocyte viability and disorganized spatial organization of T cell and B cell responses.

Having demonstrated a central role for FRCs in B cell homeostasis and humoral immunity, our findings highlight the pleiotropic nature of FRCs and suggest functional heterogeneity within this cellular compartment, which raises the concept of distinct FRC subsets in defined lymph node regions. In this context, stromal cells are thought to arise from a primordial mesenchyme in the lymph node anlagen, which initially develops into lymphoid tissue–organizer cells[38]. Colonization by B lymphocytes and T lymphocytes after birth then promotes the development of conventional stromal subsets. The similar pattern of expression of cellular markers by MRCs and lymphoid tissue–organizer cells suggests that MRCs differentiate into FRCs and FDCs and continuously supply additional stromal subsets[18]. If indeed FRCs arise from MRCs in adult lymph nodes, then the *Ccl19* promoter must be silenced in MRCs. Furthermore, our studies indicated that most FDCs were devoid of promoter activity and should thus be refractory to DTxn-induced apoptosis. A few cell processes from FDCM1^{+} cells displayed weak positivity for eYFP. However, given the tight association between FRCs and FDCs in follicles[4,32], it remains difficult to discern between true promoter activity in these FDCs and proximity to eYFP[+] FRCs in follicular regions. In this context, we observed functionally competent FDCs early after the administration of DTxn, when profound loss of FRCs had already occurred, which suggested that FDCs were not directly targeted in this system. Consequently, the decrease in staining of FDCM1 at later time points, probably mediated by contraction or de-differentiation of the FDC network, may have arisen from as-yet-unrecognized crosstalk between FRCs and FDCs. Our finding that contraction of the FDC network was transient and was rapidly followed by a regeneration phase is notable. One potential explanation for this is that damage to the FDC network, secondary to FRC loss, may induce MRCs to generate new FDCM1^{+} cells[39].

As the complexity of the cellular constituents of lymph node stroma continues to grow, understanding of their developmental origins and functional interactions remains incomplete. Our results have demonstrated heterogeneity of the FRC network and indicated functional specialization of FRCs in the T cell zone versus those in the B cell zone. BAFF[+] FRCs in follicles shared common signatures with canonical FRCs, which suggests some relationship between them. However, they differed in their localization, and we did not find BAFF-producing cells in T cell areas. As mesenchymal cells are typically highly flexible in nature, depending on the surrounding environment, it is possible that BAFF production by FRCs in the B cell zone is maintained by microanatomical cues. Several functions associated with T cell immunity have been assigned to FRCs[3–7,9,19,26,40], yet the requirement for these cells in humoral responses has not been addressed. Our finding that the homeostasis of B cells and T cells was governed by a common stromal cell expands the understanding of the stromal network and underscores its central role in immunity.

Stromal cells have long been recognized as key structural components of secondary lymphoid organs[41]. Moreover, how stromal cells interact with hematopoietic cell populations and influence adaptive immunity has been delineated[42,43]. Various pathogens have been reported to affect the stromal network in lymphoid organs of humans, nonhuman primates and rodents, and such alterations can be deleterious to host defense and vaccine responsiveness[1,44]. Here we have shown the existence of a mesenchymal cell population with FRC characteristics that supported follicle identity and B cell survival through localized production of BAFF. We anticipate that our findings may inform new approaches for boosting natural and vaccine-induced humoral immunity and for protecting against potentially devastating infections.

## METHODS

Methods and any associated references are available in the online version of the paper.

## AUTHOR CONTRIBUTIONS

V.C. and M.C.W. designed and performed experiments and analyzed results; L.O., J.Cu., J.M.N.-B., F.A.S., J.Ch., F.C. and C.J.H. performed experiments; K.W. provided reagents and critical input on the manuscript; B.L. provided *Ccl19*-Cre mice and critical input on the manuscript; M.C.C. and S.J.T. designed and supervised the study; and V.C. and S.J.T. wrote the manuscript.

## COMPETING FINANCIAL INTERESTS

1. Mueller, S.N. & Germain, R.N. Stromal cell contributions to the homeostasis and functionality of the immune system. *Nat. Rev. Immunol.* **9**, 618–629 (2009).
2. Turley, S.J., Fletcher, A.L. & Elpek, K.G. The stromal and haematopoietic antigen-presenting cells that reside in secondary lymphoid organs. *Nat. Rev. Immunol.* **10**, 813–825 (2010).
3. Gretz, J.E., Norbury, C.C., Anderson, A.O., Proudfoot, A.E. & Shaw, S. Lymph-borne chemokines and other low molecular weight molecules reach high endothelial venules via specialized conduits while a functional barrier limits access to the lymphocyte microenvironments in lymph node cortex. *J. Exp. Med.* **192**, 1425–1440 (2000).
4. Roozendaal, R. *et al.* Conduits mediate transport of low-molecular-weight antigen to lymph node follicles. *Immunity* **30**, 264–276 (2009).
5. Sixt, M. *et al.* The conduit system transports soluble antigens from the afferent lymph to resident dendritic cells in the T cell area of the lymph node. *Immunity* **22**, 19–29 (2005).
6. Acton, S.E. *et al.* Podoplanin-rich stromal networks induce dendritic cell motility via activation of the C-type lectin receptor CLEC-2. *Immunity* **37**, 276–289 (2012).
7. Astarita, J.L., Acton, S.E. & Turley, S.J. Podoplanin: emerging functions in development, the immune system, and cancer. *Front. Immunol.* **3**, 283 (2012).
8. Malhotra, D. *et al.* Transcriptional profiling of stroma from inflamed and resting lymph nodes defines immunological hallmarks. *Nat. Immunol.* **13**, 499–510 (2012).
9. Link, A. *et al.* Fibroblastic reticular cells in lymph nodes regulate the homeostasis of naive T cells. *Nat. Immunol.* **8**, 1255–1265 (2007).
10. Khan, O. *et al.* Regulation of T cell priming by lymphoid stroma. *PLoS ONE* **6**, e26138 (2011).
11. Lukacs-Kornek, V. *et al.* Regulated release of nitric oxide by nonhematopoietic stroma controls expansion of the activated T cell pool in lymph nodes. *Nat. Immunol.* **12**, 1096–1104 (2011).
12. Siegert, S. *et al.* Fibroblastic reticular cells from lymph nodes attenuate T cell expansion by producing nitric oxide. *PLoS ONE* **6**, e27618 (2011).
13. Cyster, J.G. B cell follicles and antigen encounters of the third kind. *Nat. Immunol.* **11**, 989–996 (2010).
14. Cyster, J.G. *et al.* Follicular stromal cells and lymphocyte homing to follicles. *Immunol. Rev.* **176**, 181–193 (2000).
15. Roozendaal, R. & Carroll, M.C. Complement receptors CD21 and CD35 in humoral immunity. *Immunol. Rev.* **219**, 157–166 (2007).
16. Tew, J.G., Kosco, M.H., Burton, G.F. & Szakal, A.K. Follicular dendritic cells as accessory cells. *Immunol. Rev.* **117**, 185–211 (1990).
17. Wang, X. *et al.* Follicular dendritic cells help establish follicle identity and promote B cell retention in germinal centers. *J. Exp. Med.* **208**, 2497–2510 (2011).
18. Katakai, T. *et al.* Organizer-like reticular stromal cell layer common to adult secondary lymphoid organs. *J. Immunol.* **181**, 6189–6200 (2008).
19. Chai, Q. *et al.* Maturation of lymph node fibroblastic reticular cells from myofibroblastic precursors is critical for antiviral immunity. *Immunity* **38**, 1013–1024 (2013).
20. Katakai, T. Marginal reticular cells: a stromal subset directly descended from the lymphoid tissue organizer. *Front. Immunol.* **3**, 200 (2012).
21. Buch, T. *et al.* A Cre-inducible diphtheria toxin receptor mediates cell lineage ablation after toxin administration. *Nat. Methods* **2**, 419–426 (2005).
22. Fletcher, A.L. *et al.* Reproducible isolation of lymph node stromal cells reveals site-dependent differences in fibroblastic reticular cells. *Front. Immunol.* **2**, 35 (2011).
23. Cervantes-Barragan, L. *et al.* Dendritic cell-specific antigen delivery by coronavirus vaccine vectors induces long-lasting protective antiviral and antitumor immunity. *mBio* **1**, 4 (2010).
24. Cupovic, J. *Low Avidity CD8+ T cells In Viral Infection from Neuroinflammation to Adoptive T Cell Therapy.* PhD thesis, Eidgenössische Technische Hochschule Zürich (2014).
25. Gonzalez, S.F. *et al.* Capture of influenza by medullary dendritic cells via SIGN-R1 is essential for humoral immunity in draining lymph nodes. *Nat. Immunol.* **11**, 427–434 (2010).
26. Chyou, S. *et al.* Fibroblast-type reticular stromal cells regulate the lymph node vasculature. *J. Immunol.* **181**, 3887–3896 (2008).
27. Okada, T. *et al.* Chemokine requirements for B cell entry to lymph nodes and Peyer's patches. *J. Exp. Med.* **196**, 65–75 (2002).
28. Mackay, F. & Browning, J.L. BAFF: a fundamental survival factor for B cells. *Nat. Rev. Immunol.* **2**, 465–475 (2002).
29. Mackay, F. *et al.* Mice transgenic for BAFF develop lymphocytic disorders along with autoimmune manifestations. *J. Exp. Med.* **190**, 1697–1710 (1999).
30. Gorelik, L. *et al.* Normal B cell homeostasis requires B cell activation factor production by radiation-resistant cells. *J. Exp. Med.* **198**, 937–945 (2003).
31. Garin, A. *et al.* Toll-like receptor 4 signaling by follicular dendritic cells is pivotal for germinal center onset and affinity maturation. *Immunity* **33**, 84–95 (2010).
32. Gonzalez, S.F. *et al.* Trafficking of B cell antigen in lymph nodes. *Annu. Rev. Immunol.* **29**, 215–233 (2011).
33. Bajénoff, M. & Germain, R.N. B-cell follicle development remodels the conduit system and allows soluble antigen delivery to follicular dendritic cells. *Blood* **114**, 4989–4997 (2009).
34. Alimzhanov, M.B. *et al.* Abnormal development of secondary lymphoid tissues in lymphotoxin beta-deficient mice. *Proc. Natl. Acad. Sci. USA* **94**, 9302–9307 (1997).
35. Boulianne, B. *et al.* AID-expressing germinal center B cells cluster normally within lymph node follicles in the absence of FDC-M1+ CD35+ follicular dendritic cells but dissipate prematurely. *J. Immunol.* **191**, 4521–4530 (2013).
36. Browning, J.L. *et al.* Lymphotoxin-β receptor signaling is required for the homeostatic control of HEV differentiation and function. *Immunity* **23**, 539–550 (2005).
37. Koni, P.A. *et al.* Distinct roles in lymphoid organogenesis for lymphotoxins α and β revealed in lymphotoxin β-deficient mice. *Immunity* **6**, 491–500 (1997).
38. Mebius, R.E. Organogenesis of lymphoid tissues. *Nat. Rev. Immunol.* **3**, 292–303 (2003).
39. Jarjour, M. *et al.* Fate mapping reveals origin and dynamics of lymph node follicular dendritic cells. *J. Exp. Med.* **211**, 1109–1122 (2014).
40. Yang, C.Y. *et al.* Trapping of naive lymphocytes triggers rapid growth and remodeling of the fibroblast network in reactive murine lymph nodes. *Proc. Natl. Acad. Sci. USA* **111**, E109–E118 (2014).
41. Junt, T., Scandella, E. & Ludewig, B. Form follows function: lymphoid tissue microarchitecture in antimicrobial immune defence. *Nat. Rev. Immunol.* **8**, 764–775 (2008).
42. Koning, J.J. & Mebius, R.E. Interdependence of stromal and immune cells for lymph node function. *Trends Immunol.* **33**, 264–270 (2012).
43. Malhotra, D., Fletcher, A.L. & Turley, S.J. Stromal and hematopoietic cells in secondary lymphoid organs: partners in immunity. *Immunol. Rev.* **251**, 160–176 (2013).
44. Scandella, E. *et al.* Restoration of lymphoid organ integrity through the interaction of lymphoid tissue-inducer cells with stroma of the T cell zone. *Nat. Immunol.* **9**, 667–675 (2008).

## ONLINE METHODS

**Mice.** *Ccl19*-Cre mice have been described[19]. *Rosa26*-eYFP mice (006148), *Rosa26*-DTR (iDTR) mice (007900), *Cd21*-Cre mice (006368) and OT-II mice (004194) were from Jackson Laboratory. TCR-S mice (in which CD8^{+} T cells specifically recognize coronavirus) have been described[24]. Mice were maintained under specific pathogen–free conditions in accordance with institutional guidelines and guidelines of the US National Institutes of Health and were used at 5–7 weeks of age. Experiments were conducted without blinding of researchers to sample identity, with sex- and age-matched mice used for all *in vivo* experiments. For experiments with multiple time points, mice were assigned randomly to each group. Animal studies were approved by the Research Animal Care committee of Dana-Farber Cancer Institute.

**Antibodies.** The following antibodies were used: anti-CD45 (30-F11), anti-CD31 (390), anti-PDPN (8.1.1), anti-MadCAM (MECA-367), anti-B220 (RA3-6B2), antibody to α-smooth muscle actin (1A4), anti-Thy-1 (53-2.1), anti-CD140α (APA5), anti-CD140b (APB5), anti-CD106 (429), anti-CD11b (M1/70), anti-CD11c (N418), anti-Gr1 (RB6-8C5), antibody to major histocompatibility complex class II (M5/114.15.2), anti-CD4 (RM4.5) and anti-CD8 (RM2206; all from Biolegend); anti-BAFF (121808 from R&D Systems); and anti-GFP (A10263 from Life Technologies).

**Systemic ablation of FRCs *in vivo*.** *Ccl19*-Cre mice were bred to *Rosa26*-iDTR mice to generate *Ccl19*-Cre × iDTR mice. DTR[+]Cre[+] mice that express DTR in *Ccl19*-expressing cells and DTR[+]Cre[−] control mice were given intraperitoneal injection of DTxn (8 ng per gram body weight) and were killed 12, 24, 48 or 72 h later. Ablation efficiency was assessed by flow cytometry at various time points, with a reduction in FRCs (CD45^{−}PDPN^{+}CD31^{−}) of 80–90% commonly seen by 72 h.

**Local ablation of FRCs *in vivo*.** DTR^{+}Cre^{+} mice that express DTR in *Ccl19*-expressing cells and DTR[+]Cre[−] control mice were given injection (into the footpad) of DTxn (0.5 ng per gram body weight) and were killed 72 h later. Local ablation was assessed by comparison of the ablation of FRCs in draining (popliteal) lymph nodes and nondraining lymph nodes.

**FDC ablation *in vivo*.** *Cd21*-Cre mice were bred to *Rosa26*-iDTR to generate *Cd21*-Cre × iDTR mice. For FDC-ablation experiments, 6-week-old male recipients were irradiated and then were given adoptive transfer of bone marrow from wild-type C57BL/6 mice. 6 weeks after reconstitution, mice were given intraperitoneal injection of DTxn (8 ng per gram body weight) and were killed 24 h later.

**Antiviral T cell–dependent responses.** Influenza virus was propagated and isolated as described[25]. 3 d after the administration of DTxn, mice were given adoptive transfer of $5 \times 10^6$ CFSE-labeled, purified OT-II CD4^{+} T cells by injection into the tail vein. 24 h later, mice received 20 μl viral suspension ($1 \times 10^6$ plaque-forming units) by subcutaneous injection into the footpad. Mice were killed 24 h later and popliteal lymph nodes were analyzed by flow cytometry. Activation and CFSE dilution were determined 60 h after T cell transfer. For the coronavirus experiments, DTxn was injected 72 h before adoptive transfer of T cells[23]. A total of $2 \times 10^6$ TCR-S CD8^{+} T cells were transferred by intravenous injection and, 12 h after transfer, mice were given subcutaneous injection (into both flanks) of $3 \times 10^6$ nonreplicating coronaviral particles[23]. Mice were given a second injection of nonreplicating coronaviral particles 12 h after the first injection. Lymph nodes were analyzed 72 h after the first injection of viral particles.

**Antiviral humoral responses.** 2 d after the administration of DTxn, mice received 20 μl influenza virus suspension ($1 \times 10^6$ plaque-forming units) by subcutaneous injection into the footpad. 14 days later, popliteal draining lymph nodes were collected, cryopreserved and imaged for analysis of the formation of germinal centers. Additionally, serum was collected for analysis of influenza virus–specific antibodies. For enzyme-linked immunosorbent assay (ELISA) of serum, influenza virus strain PR8 that had undergone ultraviolet irradiation was immobilized on a plate with high binding capacity, followed by the addition of collected serum and probing for specific binding of IgM or

IgG2b (Sigma) by standard alkaline-phosphatase development. For experiments involving immunization with TNP-Ficoll, mice were given injection of DTxn and, 2 d later, were given intraperitoneal injection of TNP-Ficoll (250 μg per mouse). IgM antibody titers in the blood were determined at day 8.

**Treatment with anti-CD62L and FTY720.** For blockade of CD62L, mice received one single intraperitoneal dose of anti-CD62L (200 μg per mouse; MEL-14; BioXcell). For the prevention of cell egress, mice were given intraperitoneal injection of FTY720 (1 mg per kg body weight; Fingolimod; R&D Systems) and, 4 h later, were given injection DTxn. Mice received an additional dose of FTY720 at 48 h and were killed for analysis at 72 h.

**BAFF in serum.** Serum was collected from mice 3 d after the administration of DTxn and were stored at −80 °C until processing. Soluble BAFF was measured in the serum samples at a dilution of 1:2 with a modified cytometric bead array. BD CBA Functional Beads (BD Biosciences) were activated and were coated with ImmunoPure streptavidin according to the manufacturer's instructions (Thermo Scientific). For array development, a commercial anti-BAFF ELISA kit (DY2106-05; R&D Systems) was used. Biotinylated detection antibody was incubated with 30 μl of streptavidin-conjugated bead slurry at a concentration of 3 μg/ml and was subsequently washed three times with PBS containing 3% FBS. Following overnight blockade of nonspecific binding, serum samples were incubated for 2 h with anti-BAFF beads in Multiscreen plates (Millipore). Beads were then washed three times with 3% FBS in PBS. ELISA capture antibody was used for the detection of BAFF bound to beads at a concentration of 4 μg/ml. Following 1 h of incubation, beads were washed, followed by incubation for 1 h with Alexa Fluor 546–conjugated goat anti-rat (a-11081; Molecular Probes). Beads were washed three times with 3% FBS in PBS, followed by an additional four washes in PBS alone. Fluorescence was detected on a FACSAria IIu (BD), and data were analyzed with FlowJo software.

**Enzymatic digestion of lymphoid organs.** For flow cytometry or cell culture of lymph node stromal cells, skin-draining lymph nodes from individual mice were dissected and then were incubated for 50–60 min at 37 °C in RPMI medium containing 0.1 mg/ml Dnase I (Invitrogen), 0.2 mg/ml collagenase P (Roche) and 0.8 mg/ml Dispase (Roche)[22]. Cells were collected every 15–20 min in PBS containing 2% FBS and 5 mM EDTA, with replacement of the digestion medium with fresh digestion medium. Spleens were digested similarly, and red blood cells were lysed with ammonium chloride–potassium bicarbonate (ACK) buffer before analysis by flow cytometry. Peyer's patches were collected and washed in 2 mM EDTA and 1 mM DTT in PBS for removal of the epithelium before enzymatic digestion.

**FRC culture *in vitro*.** Single-cell suspensions from pooled skin-draining lymph nodes underwent enrichment for MadCAM-1^{−} cells through the use of a biotinylated MadCAM-1-specific antibody (120706; Biolegend) and anti-biotin microbeads (Miltenyi). Cells were counted and then were plated at a density of $5 \times 10^5$ cells per cm$^2$ in αMEM supplemented with 10% FBS, 1% penicillin-streptomycin and 1% glutamine. Nonadherent cells were removed after 24 h. After 5 d, primary cultures (mainly FRCs and lymphatic endothelial cells) were harvested and then were purified by magnetic-activated cell sorting as CD45^{−}CD31^{−} cells (FRCs).

**FRC–B cell cocultures.** FRCs were purified from primary lymph node cultures (as described above) and were seeded at a density of $2.5 \times 10^5$ cells per ml in complete αMEM medium. Freshly purified lymph node B cells (B220 negative selection kit; Miltenyi) were overlaid on top of the FRC layer at a ratio of one FRC to five B cells. In some experiments, FRCs were grown on the bottom of a Transwell system chamber and B cells were added to the top of the insert. Alternatively, B cells were cultured in FRC-conditioned medium (supernatant of purified FRCs collected 5 d after seeding).

**Flow cytometry analyzing BAFF and protease inhibition.** Lymph nodes were enzymatically digested and single-cell suspensions were stained in flow cytometry buffer. FRCs were identified as being negative for staining with propidium iodide and as CD45^{−}CD31^{−}PDPN^{+}MadCAM^{−} cells. Monoclonal

antibody to BAFF (121808; R&D Systems) or isotype-matched control antibody (54447; R&D Systems) were used. For protease inhibition, cells were treated with Batimastat (25 μM in dimethyl sulfoxide; Abcam) and decanoyl-Arg-Val-Lys-Arg-chloromethylketone (25 μM in dimethyl sulfoxide; Bachem).

**Immunohistochemistry and confocal microscopy.** Isolated tissues were fixed for 2–4 h in 4% paraformaldhehyde (PFA) and were placed in 30% sucrose until saturation. Tissues were embedded in optimal cutting temperature medium, then were frozen and cut into sections 10–20 μm in thickness. Sections were immunostained (antibodies identified above) and were imaged with a Leica SP5X laser-scanning confocal microscope. All of the images with eYFP signals were counterstained with a chicken GFP-specific antibody (identified above), followed by fluorescein isothiocyanate–conjugated anti-chicken (A-11039; Life Technologies).

**Deposition of phycoerythrin-tagged immunocomplexes.** The uptake of phycoerythrin-tagged immunocomplexes by FDCs was assessed by standard confocal microscopy. At 18 h following ablation of FRCs, mice were passively immunized with 100 μg rabbit monoclonal antibody to phycoerythrin (100-4199; Rockland), followed 6 h later by subcutaneous injection of 1 μg phycoerythrin into the footpad. Popliteal draining lymph nodes were fixed in 4% PFA, cryopreserved, sectioned and imaged as described above.

**Conduit analysis.** Mice were given intravenous injection of 3 μg Alexa Fluor 568–conjugated anti-CD35 (8C12; grown in-house) 6–18 h before lymph nodes were collected. Conduit staining was achieved by subcutaneous injection of fluorescein isothiocyanate–saturated PBS solution (10 μl) into the footpad 4–6 h before popliteal lymph nodes were collected.

**Quantification of FDCs.** Popliteal lymph nodes from DTxn-treated mice were isolated and fixed in 4% PFA. Lymph nodes were equilibrated in 30% sucrose and serially sectioned. Four sections from each individual lymph node were obtained at 100-μm increments through the lymph node and then were stained for confocal microscopy (antibodies identified above). The resulting images were analyzed with CellProfiler cell image–analysis software for the identification of individual B cell follicles in each section. Fluorescence data were assessed for each follicle and then were integrated so that each lymph node data point represents at least three combined sections.

**Statistical analysis.** Two-tailed, unpaired Student's $t$-tests were used for statistical analyses, with the assumption of equal sample variance, with GraphPad Prism software. Differences with a $P$ value of $<0.05$ were considered statistically significant. Sample size was not specifically predetermined, but the number of mice used was consistent with prior experience with similar experiments.